Journal of Mining and Environment (JME) Vol. 17, No. 3, 2026, 973-991

Shahrood University of Technology

Journal of Mining and Environment (JME)

Journal homepage: www.jme.shahroodut.ac.ir

Iranian Society of Mining Engineering (IRSME)

Karst susceptibility assessment at linear infrastructure facilities using GIS and Remote Sensing in the Vladimir region, Russia

Elena Drobinina[1*], Marina Kitaeva[1], Artem Mizev[1], and Elizaveta Romanova[2,3]

1. Geology Faculty, Perm State University, Perm, Russian Federation
2. Sergeev Institute of Environmental Geoscience Russian Academy of Science, Moscow, Russian Federation
3. Moscow State University of Civil Engineering (MGSU) National Research University, Moscow, Russian Federation

Article Info

Received 29 October 2025
Received in Revised form 01 December 2025
Accepted 20 December 2025
Published online 20 December 2025

DOI: 10.22044/jme.2025.17055.3363

Keywords

GIS
Karst
Karst susceptibility
Remote sensing data
Sinkhole

Abstract

The study presents an integrated approach to karst susceptibility assessment using Geographic Information Systems (GIS) and Remote Sensing (RS) data for sinkhole mapping and spatial analysis. The approach enables rapid and reliable karst susceptibility assessment in areas where linear infrastructure has been designed within the Pivovarovo karst area (Vladimir Region, Russia). The research highlights the advantages of automated zoning along the construction route based on both sinkhole distribution and environmental conditions. A significant methodological contribution to the assessment of karst susceptibility is the development of a custom Python-based tool for the automated morphometric analysis of sinkholes, including diameter measurement and orientation assessment. This approach provides an effective solution for karst susceptibility assessment, because it enables the rapid processing of large datasets, producing high-quality results that can support engineering design decisions.

1. Introduction

The presence of dangerous geotechnical processes in built-up areas significantly complicates engineering surveys. In karst regions, it is imperative to accurately assess karst hazards to ensure the safe operation of engineering infrastructure. Karst landscapes are typified by the pervasive presence of closed depressions, which vary in size [1]. Depending on their genesis, these depressions are classified as dolines or sinkholes. A doline is defined as any topographical depression in karst terrain that functions as a funnel, thereby channeling rainfall and surface runoff vertically to recharge the karst aquifer. Conversely, the term «sinkhole» is generally employed to denote a collapsed or covered doline [2].

Collapsed sinkholes often form spontaneously, posing significant economic, environmental, and social risks. A key feature of karst is that new sinkholes emerge in proximity to pre-existing ones, where conditions conducive to sinkhole formation are already in place. This pattern underscores the relevance of detailed studies of surface karst for comprehensive hazard prediction.

Short timeframes for engineering surveys frequently result in an incomplete understanding of karst dynamics within a project area. However, contemporary spatial analysis techniques in Geographic Information Systems (GIS), in conjunction with the accessibility of Remote Sensing (RS) data and a comprehensive array of spatial data analysis tools, now facilitate expeditious and exhaustive karst investigation [3].

The potential of GIS and RS extends far beyond the scope of karst studies, with critical applications in the assessment of a wide spectrum of environmental risks. A compelling example of this

Corresponding author: alenadrobinina@yandex.ru (E. Drobinina)

is wildfire management, where these technologies are indispensable for modelling fire probability. As demonstrated in a study of the protected areas of Mayurbhanj District (India), an integrated approach using multi-criteria decision models (AHP/FAHP) with variables such as vegetation type, climate, topography, road buffer and historical MODIS fire data can accurately delineate high-risk zones [4].

Geospatial technologies demonstrate universal applicability across diverse environmental domains. For instance, a Punjab groundwater study used 26-year data to reveal a dramatic water table decline from 3.6 to 30.7 meters, enabling precise drought risk zoning [5].

In the scientific community, advanced statistical and machine learning techniques – including frequency ratio, logistic regression, and artificial neural networks – are now considered standard practice for modelling landslide susceptibility. These methods leverage geospatial data, including digital elevation models, lithology, and land use, to effectively identify high-risk areas based on critical conditioning factors such as slope, aspect, and geology [6]. To illustrate this point, consider the example of a landslide risk assessment in Lahaul and Spiti, India, which employed multiple machine learning models. In this instance, the Random Forest model was identified as the most effective model (AUC = 0.954). The study revealed high-risk zones, primarily due to slope and river proximity, providing critical data for infrastructure protection [7]. To further illustrate this point, a landslide susceptibility study in Spiti Valley, India, demonstrated that advanced machine learning and new sampling procedures (Buffer Zone Safe Points and Slope Buffer Safe Points) may improve the accuracy of landslide susceptibility mapping and reliability in high-risk zones. In order to facilitate a comprehensive comparison of their predictive capabilities, detailed landslide susceptibility zonation maps were generated using three advanced machine learning techniques. The following machine learning algorithms were employed: extreme gradient boosting (XGBoost), random forest (RF), and K-nearest neighbors (KNN) [8, 9, 10]. Another notable example is that of landslide susceptibility mapping in the Himalayas, where Frequency Ratio and Information Value models achieved high predictive accuracy (AUC $\approx$ 0.84). The study, which was validated against over 1,000 landslide events, successfully classified terrain into five risk categories. This demonstrates the practical value of geospatial analysis for infrastructure protection and disaster preparedness in mountainous regions [11].

A final compelling illustration of the universal applicability of geospatial technologies is found in the management of urban air quality. Research in Delhi (2018-2023) used GIS-based Kriging interpolation and statistical analysis to model the spatial and temporal dynamics of major pollutants, effectively quantifying the drastic reduction in major pollutants during the lockdown imposed due to the global pandemic, known as «Coronavirus Disease 2019» (Covid-19). This approach facilitated the generation of a high-resolution visualization of pollution patterns, thereby directly correlating emission sources with air quality impacts and providing a data-driven foundation for the development of public health policy. The efficacy of this methodology in a complex urban environment underscores a critical paradigm: the integration of spatial interpolation, time-series analysis, and statistical validation within a GIS framework provides a powerful, transferable model for environmental assessment [12]. This reinforces the broader perspective that advanced geospatial analytics – whether applied to atmospheric pollution, wildfires, landslides, or karst – represent a unified and indispensable toolkit for modern environmental risk assessment and sustainable territorial planning.

The article is to address significant aspects of enhancing surface karst investigation in areas, where linear infrastructure designed. The primary objective of this study is to automate the process of surface karst analysis with a view to improving the accuracy of karst susceptibility assessment and optimizing the time required for its execution. The demonstration is provided of the use of remote sensing data and modern spatial analysis tools, including automated procedures developed in Python for GIS, to improve the quality and efficiency of karst research. This integrated approach facilitates rapid and accurate analysis of the karst process, enabling the measurement of karst forms and zoning territory. Consequently, it supports strategic planning and risk mitigation for engineering projects in karst terrain.

The research focuses on the Pivovarovo karst area in the Vladimir Region of Russia. The Pivovarovo karst area is distinguished by a significant development of sinkholes. The occurrence of sinkholes in this region has been thoroughly documented and verified through field research. This prior validation enables a robust assessment of the proposed methodology, allowing

for direct comparison between remote sensing and GIS-based evaluations and established field data.

2. Sinkhole identification and mapping

A conventional methodology for the evaluation of surface karst typically entails the use of satellite imagery for the identification and mapping of sinkholes, followed by the compilation of a comprehensive catalogue. Such a catalogue contains parameters for each form, including spatial location, dimensions (length, width, area, radius, depth), temporal changes (if monitoring data are available), date of formation (if known), and other parameters specific to the research objectives. The mapping and vectorization of karst sinkholes using panchromatic and multispectral satellite imagery is still predominantly performed manually [13].

The use of remote sensing data for the identification of sinkholes is an established practice. For instance, a study collated a catalogue of sinkholes across an area exceeding 5 million hectares using remote sensing data. In this research, 398 potential karst forms were identified on a section of the Central Anatolian Plateau in Turkey. The identification process involved the use of high-resolution satellite imagery, aerial photographs, and a Digital Elevation Model (DEM). A further 100 karst forms were documented on the basis of archival materials and published literature. The location and geometry of these forms were subsequently verified using GPS and total stations, confirming 283 sinkholes in the study area. The development of a dedicated application for field verification of forms identified through satellite imagery interpretation proved to be a highly valuable addition to the research methodology [14].

The use of remote sensing data in karst studies has expanded beyond the confines of traditional satellite imagery analysis. Researchers now routinely employ DEMs to identify local depressions, enabling semi-automated interpretation of satellite data within GIS environments. In karst terrains, where groundwater interacts closely with surface water through specific hydrological and geomorphological features, DEMs have proven particularly valuable. This relationship has facilitated the creation of aquifer vulnerability maps [15] based on DEMs and surface karst distribution patterns. Furthermore, DEMs provide critical data for hydrological modelling of surface runoff and groundwater recharge [15], delineation of protection zones for wells and springs [17], and modelling of pollution pathways [18, 19]. A significant methodological advancement pertains to the hydrological correction of DEMs for sinkhole identification, wherein researchers detect negative, closed, rounded relief features – specifically drainless depressions genetically linked to karst [19, 20, 21].

Building on these advancements, several authors have proposed semi-automated methods for karst sinkhole detection using digital elevation models derived from interferometric synthetic aperture radar (IFSAR-DEM). These approaches generally incorporate hydrological modelling techniques – including watershed delineation and sink-fill algorithms – to identify depression features and measure sink depths. The detected depressions are subsequently classified and validated using supplementary data sources such as Google hyperspectral imagery and contemporary DEMs [22].

In recent years, there has been considerable progress in the development of automatic detection methodologies for various types of karst depression, employing a range of digital elevation model. Research indicates that laser scanning data (LiDAR) is particularly efficacious for the automated identification of karst depressions due to its high spatial resolution and capacity to penetrate vegetation cover [22, 23, 24, 25].

To streamline the manual digitization of depressions from DEMs, researchers employed the Red Relief Image Map (RRIM) visualization technique. The integration of three topographic parameters – slope, positive openness, and negative openness – serves to accentuate elevations and depressions, respectively. The input data, supplied by the Turkish General Directorate of Mapping, comprised the following: aerial photographs, satellite imagery, a 10-m contour interval topographic map, and a 5-m resolution DEM. The positive and negative openness layers were processed using SAGA GIS and subsequently utilized to compute the Ridge and Valley Index (RVI). The final RRIM output is effectively represented by the combination of this index and topographic slope data, whereby topographic convexities and concavities are represented as elevations and depressions, respectively. This methodology enhances manual identification of karst depressions by shading side slopes while highlighting karst form boundaries [26].

A comparable approach was applied to airborne LiDAR-derived digital terrain models in Austria. Despite the study's primary focus on the

visualization of digital terrain models for archaeological feature mapping, the author emphasized its efficacy in differentiating topographic elements, including elevations and depressions [27].

In addition to the manual digitization of sinkholes, the delineation of such features can be enhanced by the use of indirect indicators. For instance, the use of spectral vegetation indices has been demonstrated to be effective in this regard, particularly when capitalizing on the characteristic shrub cover typically found on the slopes and bottoms of karst sinkholes [28].

The resulting sinkhole dataset is used as fundamental input for various spatial analyses. These include density-based territorial zoning, as well as the construction of histograms for sinkhole diameters or environmental factor distributions. These analyses are of crucial importance in the development and validation of predictive karst models [29, 30]. A pertinent example is a study in which a karst hazard map was generated using subsurface karst data combined with the thickness and lithology of overlying soils. The study area was classified into three hazard classes, and subsequent validation against known sinkhole locations revealed an absence of sinkholes in low-hazard class territory, thus confirming the accuracy of the karst hazard delineation criteria [31].

The practical utility of surface karst mapping thus lies in its dual efficiency for both karst hazard assessment and environmental zoning. This is of particular concern given that karst formations frequently act as direct conduits for pollutants into underground aquifers [19].

3. Sinkhole diameter measurement

The measurement of sinkhole diameter can be achieved through a variety of methodologies, including manual, semi-automated, and automated approaches. The utilization of high-resolution satellite imagery or digital elevation models facilitates the identification of sinkholes.

The Manual Method. Popular mapping services such as Yandex Maps, 2GIS, and Google Maps provide access to high-resolution satellite imagery with built-in surface distance measurement tools. These platforms have been found to be suitable for preliminary surface karst analysis, allowing users to determine sinkhole diameters, distances from objects of interest, and mutual locations. The primary benefits of these tools are twofold: firstly, they can be accessed without the need for additional software installation, and secondly, they are compatible with mobile devices. However, the system is not without its limitations, which include the absence of built-in tables for saving results, the inability to perform statistical analysis, and impracticality for large-area measurements. Google Earth Pro offers enhanced functionality by enabling high-resolution image viewing, manual sinkhole delineation, and saving digitization results in vector formats (e.g., KMZ) for subsequent GIS-based size measurements.

The Semi-Automated Method. This approach employs standard GIS software (e.g., QGIS, ArcMap, NextGIS) in a step-by-step manner to create, edit and visualize geospatial information. The software provides extensive tools for the processing of both vector and raster data. The method involves the generation of a minimum bounding surface, where the width corresponds to the maximum sinkhole diameter, and the length corresponds to the minimum sinkhole diameter. The surface typically forms a rectangle with an inscribed circular or elliptical shape – sinkhole. While this method is efficient for rapid measurement of multiple sinkholes, it lacks high accuracy, as the rectangle's orientation may not align with the sinkhole's major axis, especially for irregularly shaped features. Nevertheless, the length of the bounding rectangle may serve as an indicator of sinkhole orientation. This method successfully circumvents the limitations of manual approaches. It has been effectively employed, for instance, in measuring depression sizes of various origins in the Araguaia Plain (Brazil) [32].

The Automated Method. In GIS environments, multiple analytical steps can be integrated into a command chain using Model Builder, allowing full execution with different input datasets at a later stage. Irrespective of the complexity or number of steps, the model functions as a unified algorithm, thus saving time and effort while minimizing errors resulting from repeated user intervention. Consequently, the sequential construction of bounding shapes and parameter calculations can be consolidated into a single tool. Users are required to provide sinkholes as input vector data, and in return they receive output with diameter values for circular shapes or major/minor axis values for elliptical shapes. This process serves to streamline the measurement process as a whole.

4. Research area

The study focuses on the Pivovarovo karst area in the Vladimir region of Russia. Despite the considerable depth of the roof of the soluble rocks,

karst processes are still active and are accompanied by the formation of sinkholes of varying diameters. The research area is characterized by a covered sulfate-carbonate karst type, as determined by the lithological composition of the soluble rocks and the thickness and lithology of the overlying soils.

One of the largest documented sinkhole collapse events occurred in 1959 on the northeastern side of a pre-existing ancient sinkhole. The initial diameter of the sinkhole was 18 meters (Figure 1); it has since expanded to 75 meters in diameter and 22 meters in depth [33]. Furthermore, reactivation of karst at the periphery of the ancient sinkhole was also observed in 2016 (Figure 2). Another sinkhole formed in the Pivovarovskoye karst field in 2016, approximately 1.5 km northwest of the previously described sinkholes (Figure 3). The recent sinkhole first appeared in November 2015. Its dimensions are 18.0 × 22.4 m in diameter, and it is 20 m deep. The sinkhole has precipitous, undrained slopes that expose clays from the Urzhumian stage of the Biarmian division (Permian system).

The Pivovarovskoe karst area is located in a sparsely populated area; therefore, the formation of sinkholes has posed limited societal or economic risk. Nevertheless, the prevalence of surface karst features has been demonstrated to engender considerable complexity with respect to the economic development of the region. Consequently, it was necessary to design a linear infrastructure route that bypasses the Pivovarovsky area to avoid substantial damage during both construction and operation.

In terms of its structural-tectonic position, the territory is situated within the Oksko-Tsinskiy Swell, classified as a fourth-order tectonic structure, and the Moscow Syncline, categorized as a third-order tectonic structure. The Pivovarovsky karst area lies within the pre-glacial Oksko-Tsinsky swell, a region characterized by gently undulating topography. Overlying this landscape are glacial sediments from the Dnieper glaciation, which have been subsequently modified through denudation processes. These processes are associated with the Suvoroshch River, which flows northeast of the site, and its tributaries particularly the Sukhodol River.

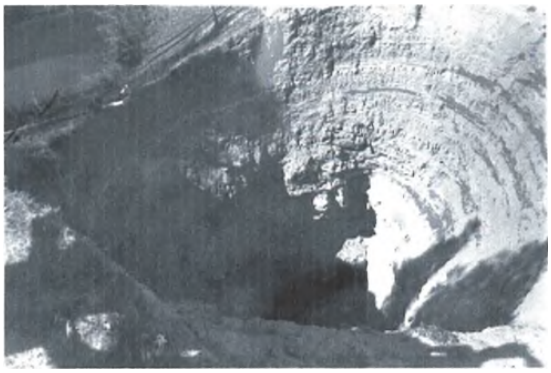

Figure 1. Archive image of the sinkhole [33]

Figure 2. Reactivation of karst at the periphery of the ancient sinkhole

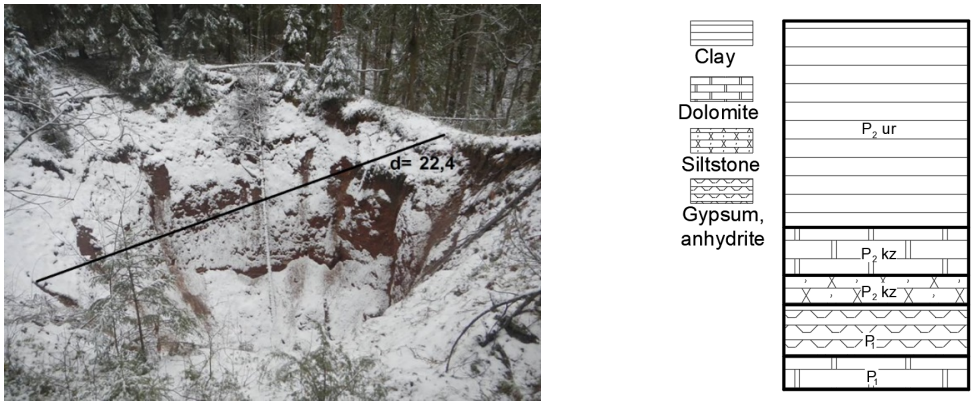

(a) **(b)**

Figure 3. Karst sinkhole (a) and typical geological section of the research area (b)

The geological structure comprises Quaternary, Triassic, and Permian deposits. The Permian stratigraphic system includes gypsum, anhydrite, limestone, and dolomite, with interlayers of clay and siltstone, dipping northeast. Overlying these are Triassic terrigenous sediments, which are widespread in the northeastern part of the study area. The uppermost part of the geological section consists of Quaternary deposits of predominantly fluvioglacial, glacial, and alluvial origin, with less common bog deposits and peats, mainly composed of sands and loams.

Karst are active within the Permian sulfate deposits. The majority of surface karst forms are cover-collapse sinkholes, with fewer occurrences of cover-subsidence and suffusion sinkholes. The formation of cover-collapse sinkholes in the area is the result of the sudden gravitational displacement of overlying terrigenous sediments into cavities within the Permian gypsum.

Morphometric analysis has revealed distinct characteristics for different sinkhole types and ages. Ancient cover-collapse sinkholes range in diameter from 5.1 to 97.4 meters (average: 25.5 m) with depths of 1–15 meters, while young cover-collapse sinkholes measure 2.5–61.5 meters in diameter (average: 18.9 m) with depths of 0.5–20 meters. Cover-subsidence sinkholes are characterized by smaller dimensions, with ancient features ranging from 2.5 to 60.1 meters in diameter (average: 14.2 m) and depths of 0.2–4.5 meters. In contrast, young features measure 2.5–12 meters in diameter (average: 4.6 m) and have depths of 0.5–3 meters. Suffusion sinkholes, which are less common, appear as closed depressions ranging from half a meter to several meters in diameter.

The vector dataset of karst sinkholes was compiled from multiple data sources. The identification and mapping of sinkholes was facilitated by the use of high-resolution satellite imagery, complemented by multispectral data analysis. In this analysis, spectral indices proved instrumental in the detection of indirect indicators of sinkhole distribution. The analysis was further enriched by the incorporation of archival and field karst survey data.

5. The surface karst assessment

The foundation for quantitative karst assessment was laid in the 1980s, when V.V. Tolmachev proposed a statistically-based method for estimating karst risk during engineering surveys and design. This approach is dependent on the Poisson distribution in order to calculate the probability of a specific number of sinkholes forming within a fixed time frame. This is based on the assumption that events occur at a known constant rate and independently of one another. The key parameter in this model is the intensity of sinkhole formation, which determines the number of sinkholes formed per unit area in one hundred years. Tolmachev emphasised the necessity of contemplating the service life of engineering structures when employing this statistical method [34, 35]. It is generally accepted that the service life of the item is 100 years. S.G. Gordienko and Yu.Yu. Savelyeva have built upon this foundation and used long-term monitoring data to apply and refine this approach [36]. Selina Z.V. and Kovaleva T.G. employed the approach to forecast sinkhole formation probabilities [37].

Quantitative evaluation of karst hazard typically relies on metrics such as sinkhole density and the sinkhole area coefficient [38]. The calculation of these parameters, which are essential for engineering design, requires accurate data on the number and size of sinkholes within the research area.

The most straightforward method of visualizing the spatial distribution of sinkholes is to create a density map, illustrating the number of sinkholes per unit area. The present study generated such a map using the «Kernel Density» tool in ArcMap 10 (see Figure 4). This technique, which is occasionally classified in literature as a semi-quantitative or hybrid method [39], calculates point density around each cell of an output raster within a specified search radius, thereby effectively implementing a moving window algorithm. An alternative methodology involves the overlaying of a grid of a predetermined size onto the study area, the counting of sinkholes within each grid cell, the interpolation of values between grid cell centroids, and the normalization of the results by the area of each cell to produce a continuous density surface.

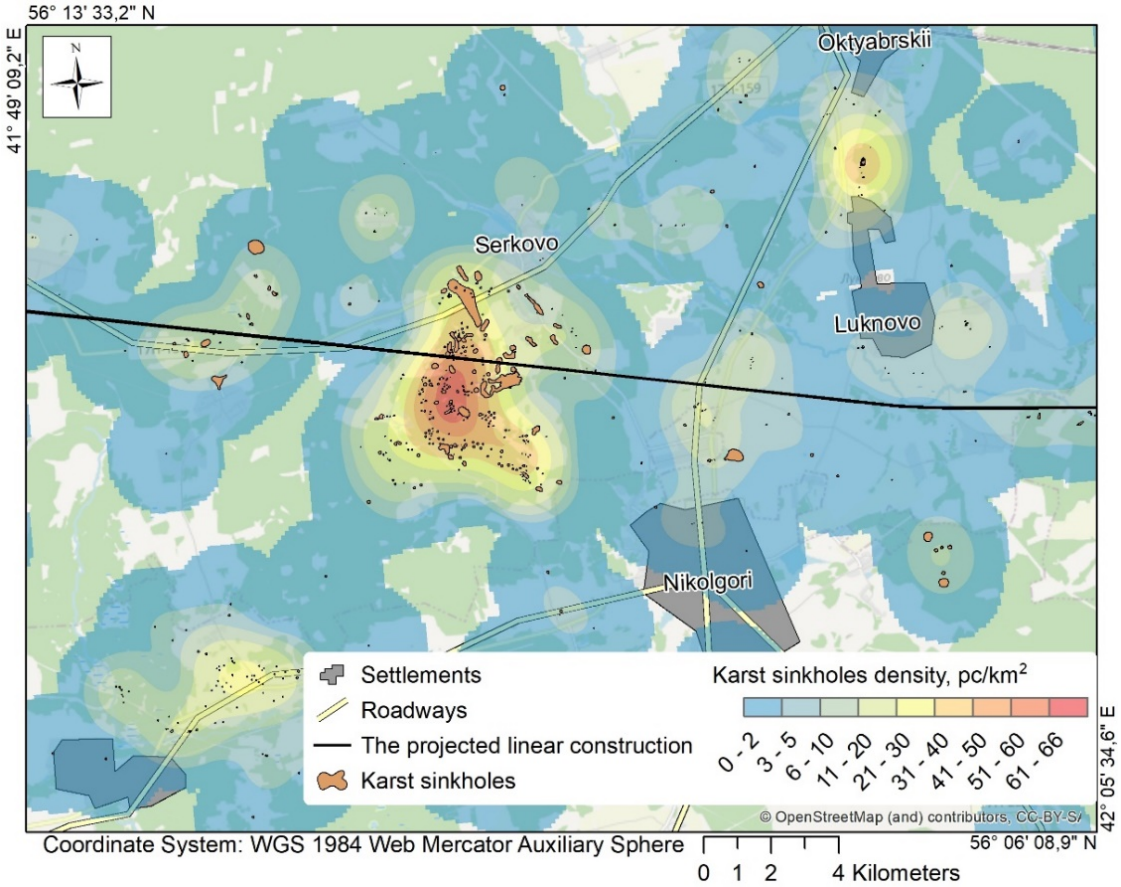

Figure 4. Density map of sinkholes

5.1. Two types of zoning of the linear construction territory and its automatization

The zoning of linear construction projects in karst regions can be categorized into two primary types. The first type is predicated on the spatial relationship between the construction and existing karst sinkholes. This zoning type is designated as «automated zoning based on sinkhole proximity». The second type is concerned with the environmental conditions of the territory that influence karst process development. This latter approach delineates conditionally homogeneous areas where karst activity takes place uniformly and sinkholes form through coherent mechanisms. This zoning type is designated as «automated zoning based on environmental conditions».

5.1.1. Automated zoning based on sinkhole proximity

A review of historical observations indicates a tendency for sinkholes to cluster in specific areas, known as karst fields. Furthermore, sinkhole density has been shown to decrease as distance from existing sinkholes increases [40]. This principle has been used by Russian scientists to forecast karst hazards in areas adjacent to known sinkholes [41], and was once incorporated into regulatory standards [42].

The distance-based assessment is implemented through the use of buffer zones of specified dimensions, generated from sinkhole edges or centroids. The buffer radii are generally established as multiples of a modular distance that is determined by mapping scale [40]. The present study employed a custom GIS tool developed for ArcMap 10 to perform karst hazard zoning along linear construction routes using this proximity-based methodology. The tool under consideration is employed to construct buffers from sinkhole edges, thereby facilitating the execution of hazard zoning along the pipeline route. The result is the identification of various categories, with different degrees of karst hazard, as demonstrated by Figure 5.

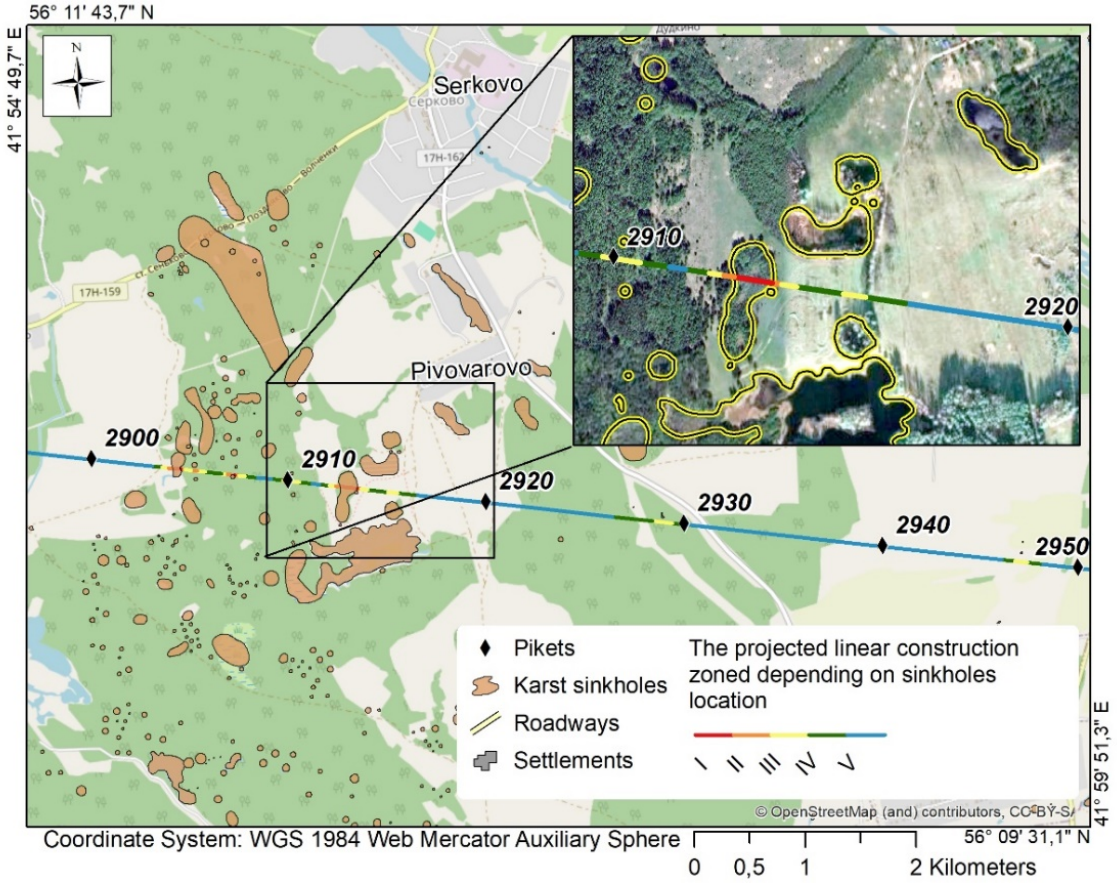

Figure 5. Karst hazard zoning map of the linear construction site based on sinkhole proximity

The zoning categories were established in accordance with the classical recommendations of Savarensky [40]. Consequently, Category I designates areas where the construction route directly intersects sinkholes. The second category is comprised of areas within a radius of 0–20 meters from sinkholes, which correspond to the minimum diameter of sinkholes classified within the highest risk category [42]. Category III encompasses distances of 20–50 meters, Category IV 50–100 meters, and Category V extends beyond 100 meters from sinkholes.

Application of the zoning tool revealed that the majority of the planned linear construction route falls within Category V, indicating relatively low susceptibility to new sinkhole formation. In contrast, categories IV through II demonstrate significantly higher karst susceptibility, as evidenced by the frequent development of new sinkholes within or in the vicinity of karst fields. This phenomenon is indicative of the presence of all necessary conditions for sinkhole formation in these zones, where karst forms enhance surface water permeability and promote karst activity. The distribution of the linear construction length across these karst susceptibility categories is detailed in Table 1.

Table 1. Areas of the linear construction territory depending on sinkhole proximity

Karst susceptibility category	Category description	Lengths of linear part of engineering construction, meter
I	the linear construction crosses a sinkhole	354.8
II	the linear construction is 0–20 meters away from a sinkhole	206.2
III	the linear construction is 20–50 meters away from a sinkhole	677.5
IV	the linear construction is 50–100 meters away from a sinkhole	1647.7
V	the linear construction is 100 meters and more away from a sinkhole	169377.5

The integration of spatial analysis and process automation facilitates rapid karst susceptibility zoning while minimizing errors associated with manual methods. Furthermore, the application of remote sensing data interpretation or archival analysis during the planning phase enables a preliminary karst assessment, providing crucial insights for potential modifications to the project.

5.1.2. Automated zoning based on environmental conditions

In the context of large linear infrastructure projects, it is imperative to undertake a definitive assessment of karst susceptibility, taking into account the inherent heterogeneity of karst massifs. The delineation of homogeneous zones is based on environmental conditions, with key factors influencing karst development, including geomorphological and geological parameters [43]. This approach enables the unambiguous determination of the prevailing sinkhole formation mechanisms within each delineated zone.

The implementation of environmental factor-based karst zoning has been noted by many scientists as having been successful. To illustrate this point, one may consider the application of machine learning algorithms in generating a karst susceptibility map for northern Guangxi, China, a map which incorporates multiple geomorphological and geological factors [44]. In a similar manner, a karst ground subsidence susceptibility map for Wuhan City was developed using the AHP–Comprehensive Index Method, integrating karst characteristics, overburden properties, and hydrodynamic conditions [45]. Comparable methodological approaches are effectively applied in assessing other geological hazards, such as landslide susceptibility, where specific combinations of natural factors determine hazard distribution [46].

The conceptual framework underpinning our karst zoning methodology draws upon the theoretical frameworks of engineering geological zoning that were established in the mid-20th century in Russia. The conventional taxonomy recognizes three zoning types: regional, typological, and mixed. The concept of regional zoning involves the application of hierarchical taxonomic units, which are categorized into regions, districts and sites. These units are distinguished by structural-tectonic criteria, characterized by the homogeneity of geological structures and the intensity of exogenous processes, respectively [47]. Typological zoning is predicated on the identification of characteristic settings based on predominant engineering geological features, while mixed zoning incorporates elements of both approaches [48].

Furthermore, a comparative-evaluative approach is employed, taking into account environmental conditions and hierarchical taximetrics units. The classification of karst areas represents a specialized type of geological zoning that exceeds the limitations of conventional classification schemes. Whilst the research is most closely aligned with the comparative-evaluative approach, it incorporates elements of both regional and typological zoning. This constitutes a distinct form of prognostic evaluation specifically adapted for karst susceptibility assessment [49].

In the research, multifactorial zoning has been implemented, incorporating the following factors:

- ✓ Tectonic unit and neotectonics factors, such as lineament density and lineament intersections, which have been identified as indicators of zones with enhanced fracturing [50].
- ✓ Geological setting, including the depth to soluble deposits and the lithological composition of overlying soils and soluble rocks.
- ✓ Geomorphological setting, that characterized by confinement to specific geomorphological elements.

The research area was systematically zoned through a hierarchical approach using ArcMap 10, in accordance with the methodological principles outlined above. The classification system is divided into three levels:

- ✓ Region, that based on the tectonic unit and neotectonics factors;
- ✓ District, that defined by the geological setting;
- ✓ Area, that determined by the geomorphological setting.

This multi-level zoning system enabled a comprehensive assessment of karst susceptibility across different spatial scales while maintaining consistency with theoretical foundations of engineering geological zoning.

The use of environmental factors was not employed directly in the determination of karst susceptibility; rather, they were utilized for the identification of quasi-homogeneous areas, the surface karst susceptibility of which was

subsequently assessed. The specific environmental factors applied in the delineation of these homogeneous karst terrain units are outlined in Table 2. Consequently, karst terrains that were quasi-homogeneous with respect to these environmental factors were identified (Figure 6).

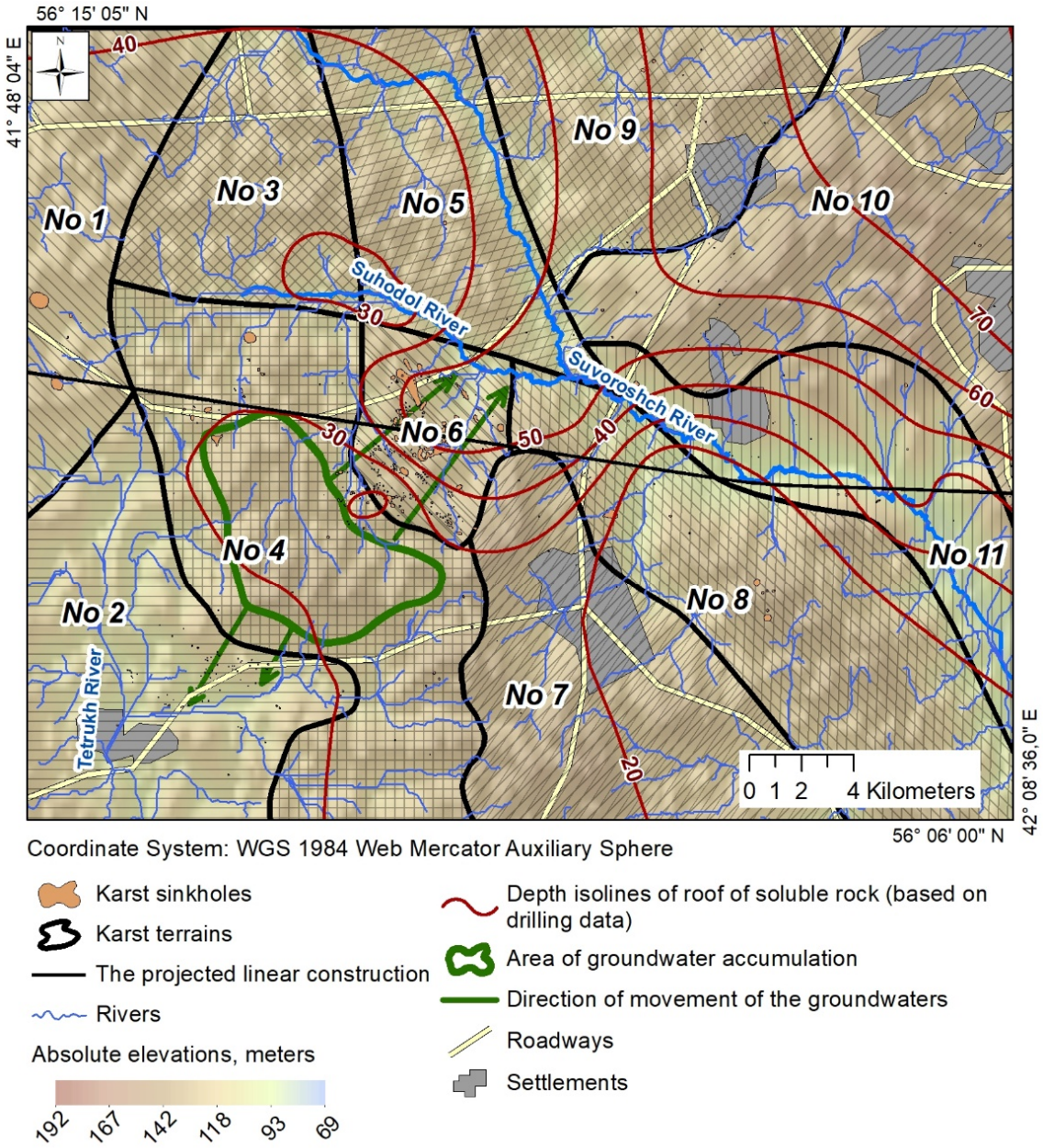

Figure 6. Map of karst terrain and associated environmental conditions

Table 2. Factors for identification of homogeneous karst terrain units

Environmental conditions										
Tectonic setting		Geology setting				Hydrogeological conditions Depth to the water table, meter Depth of water table stabilization, meter			Geomorphological setting	Karst terrain
Tectonic unit	Neotectonic activity	Overlying soils lithology	Overlying soils thickness, meter	Bedrock clay (indurated) thickness, meter	Soluble rocks lithology	Quaternary aquifer	Bedrock clay aquifer	Karst aquifer		
Oksko-Tsninsky Swell	low	Sand with loam interbeds (Q); Indurated clay (P_2)	30-32	20-23	Limestone and dolomite (P_1-P_2)	No aquifer present	No aquifer present	30-32 no data	Watershed between the Suvoroshch and Tara Rivers (right tributaries of the Klyazma River, Oka River basin). Elevations: 110-135 meters	**No 1**
	medium								Valley of the Tetrukh River (left tributary of the Kolp River, Oka River basin). Elevations: 96-130 meters	**No 2**
	low		24-32	21-30	Limestone and dolomite (P_1-P_2); Gypsum (P_1)		7-20 7-20	24-60 7-28	Watershed between the Suvoroshch River and its right tributary, the Sukhodol River. Elevations: 110-135 meters	**No 3**
	high								Right bank of the Suvoroshch River, upstream of the Sukhodol River confluence. Elevations: 95-120 meters	**No 5**
	medium								Right bank of the Suvoroshch River, downstream of the Sukhodol River confluence. Elevations: 93-144 meters	**No 8**
	high		42-54	40-51			34-46 21-26	34-46 21-26	Right bank of the Sukhodol River, downstream of the Sukhodol River confluence. Elevations: 100-138 meters	**No 6**
	low	Indurated clay (P_2)	24-26	24-26			No aquifer present	24-26 no data	Left bank of the Tetrukh River. Elevations: 105-144 meters	**No 4**
	medium								Watershed between the Tetrukh and Sukhodol Rivers. Elevations: 123-150 meters	**No 7**
	medium	Loam with sand interbeds (Q); Indurated clay (P_2)	40-42	36-38			7-8 7-8	70-73 9-10	Right bank of the Suvoroshch River, upstream of the Tyuryakha River confluence (left tributary of the Suvoroshch River). Elevations: 103-150 meters	**No 9**
	low								Valley of the Suvoroshch River. Elevations: 120-150 m	**No 10**
	medium		60-90	25-90	Dolomite (P_1); Gypsum (P_1)	3-13 3-13	38-66 no data	No aquifer present	Right bank of the Suvoroshch River, watershed between the Suvoroshch River and its tributary, the Tyuryakha River. Elevations: 89-120 meters	**No 11**

The delineated karst terrains exhibit distinct levels of karst susceptibility. The highest sinkhole density (21.2 per km2) was demonstrated within karst terrain No. 6, while the lowest (0.3 per km2) was demonstrated within karst terrain No. 3. The occurrence of concentrated sinkholes within karst terrain No. 6 is attributable to a number of interacting factors. These include the presence of well-developed horizontal and vertical relief dissection in the southwestern vault section of the structural element, a phenomenon which facilitates karst aquifer recharge. This is complemented by the northeastern dip of strata of soluble rocks, which provides natural drainage towards the Suvoroshch River valley.

In order to facilitate the zoning of linear infrastructure, the authors developed a specialized tool that rapidly identifies boundary stations (pickets), thus eliminating human error. The output comprises a comprehensive table correlating each karst terrain with corresponding linear construction segments and their respective stationing (pickets, Table 3). This rapid route segmentation capability significantly simplifies the design of karst protection, whose cost and specifications are directly determined by localized environmental conditions along the route.

Table 3. Areas of the linear construction territory depending on environmental conditions

Karst terrain number	Lengths of linear part of engineering construction, meter	Karst sinkholes density, pcs/km^2	Pikets
1	2398.7	0.4	2824+74.3-2848+73.0
4	4879.2	1.5	2848+73.0-2897+60.4
6	3323.4	21.2	2897+60.4-2930+72.5
8	4485.8	0.8	2930+72.5-2975+55.1
10	463.9	1.3	3036+56.5-3041+18.2
11	6104.7	1.4	2975+55.1-3036+56.5

5.2. Automation of sinkhole diameter estimation

The diameter is a pivotal morphological parameter of sinkholes, which has traditionally been measured manually, particularly in the case of irregularly shaped features. In this study, the authors employed an automated approach to measure circular sinkhole diameters and the major and minor axes of elongated sinkholes, while also determining the orientation of the major axis for elongated ones.

The focus on elongated sinkhole orientation is methodologically justified, as sinkholes are often structurally controlled by fracture zones and concentrated within lineament axial parts. A predominant orientation trend of sinkholes enables the general fracturing direction within the karst massif to be inferred.

Lineament analysis in the Perm Krai karst area – encompassing both sulfate (Kungur, Polazna settlement) and carbonate (Kizelovskaya anticline, Ufimskoe plateau) rock terrains – has demonstrated that surface and subsurface karst forms correlate with lineament axial zones. These zones exhibit elevated fracturing and permeability, whereas karst form density is minimal in massive, low-fracture rock units [51, 52].

For the purpose of automated sinkhole diameter estimation, the authors developed a specialized calculation tool that integrates a custom algorithm developed in the Python programming language. The tool operates as a «black box», performing intermediate calculations transparently and presenting users with the final results. The algorithm identifies the geometric centroid of each sinkhole polygon and measures ray lengths from the centroid to the polygon edge at 1-degree intervals clockwise from north. The maximum and minimum radii are determined through a comparison of sequential ray lengths (Figure 7), with the corresponding values and axis azimuths automatically recorded in the attribute table. This automated approach has been shown to significantly reduce processing time, enhance measurement accuracy, and support efficient, repeatable analysis of large sinkhole datasets.

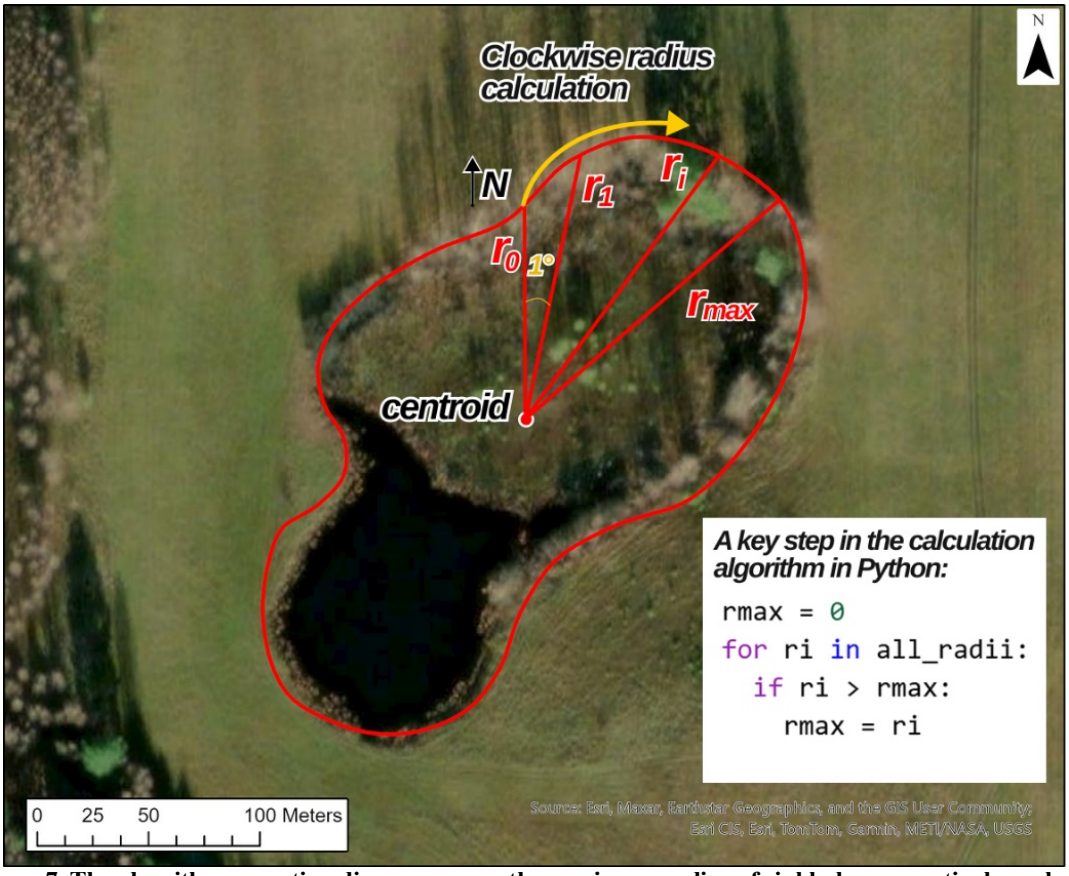

Figure 7. The algorithm operation diagram: r_{max} – the maximum radius of sinkhole, r_i – particular value of sinkhole radius, r_0 – first measured value of sinkhole radius, N – the direction to the north (for first measurement), *all_radii* – all measured sinkhole radii

The automated sinkhole morphometry assessment generates a detailed catalogue of sinkholes. Following the implementation of zoning based on environmental conditions, histograms depicting the distribution of sinkhole diameters (Figure 8) and rose diagrams illustrating the orientation of sinkhole axes (Figure 9) were generated for karst terrains.

The tool demonstrates a high degree of accuracy, as evidenced by a comparison with field karst survey data. The calculated values for the major axis demonstrated an 85-97% match with field measurements, while the minor axis exhibited an 80-100% match. The deviation from field-measured values did not exceed three meters in total.

The distribution of sinkholes by average diameter serves as a highly informative characteristic for each karst terrain. Given the influence of multiple factors on sinkhole sizes, the diameter distribution within a specific karst terrain enables the determination of their normative values. These are defined as the most representative sinkhole diameters that are characteristic of that particular karst area.

The analysis of chart data indicates that the majority of sinkholes are located within the 10–20-meter diameter range. Additionally, there is a notable presence of sinkholes in the 0–10-meter and 20–30-meter diameter ranges. In general, the distribution pattern of karst terrain No. 6 (Figure 8b) is similar to that of the entire Pivovarovsky karst area (Figure 8a). This is because it contains the largest number of sinkholes and serves as the reference dataset for constructing distribution histograms across the entire study area. However, a comparative analysis reveals an asymmetry towards smaller diameters throughout the Pivovarovsky karst area as a whole.

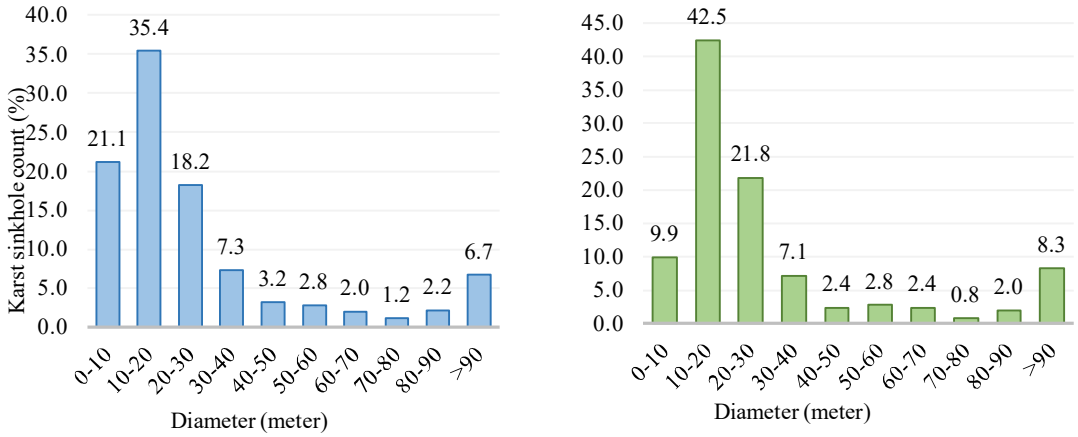

(a) (b)

Figure 8. Distribution of sinkholes by their diameters: for the Pivovarovsky karst area (a), for karst terrain No. 6 (b)

The use of automated calculation techniques offers many advantages, including the ability to estimate diameter with great precision and speed up the processing of large sinkhole datasets. Analysis of the Pivovarovsky karst area, which comprises 507 sinkholes, revealed a morphological classification based on major-to-minor axis ratio. Sinkholes with ratios below 1.2 were categorized as round (approximately 75%), while those with ratios of 1.2 or greater were classified as oval.

This automated methodology allows for the incorporation of a novel parameter in surface karst assessment: sinkhole orientation. The alignment of major axes has been demonstrated to indicate the direction of sinkhole elongation, which may reflect the principal fracturing orientation within the karst massif. The efficacy of rose diagrams in visualizing directional patterns has been demonstrated, as illustrated for both the entire Pivovarovsky karst area and the karst terrain No. 6 (Figure 9).

It is noteworthy that the orientation of sinkholes in karst terrain No. 6 is aligned with the course of the Suvoroshch River, which is the region's primary waterway. This correlation suggests that fracture patterns influencing sinkhole formation may parallel structural features expressed in the landscape. Furthermore, the northeastern dip of the soluble rock strata could reveal fracture systems oriented perpendicular to the dip direction, analogous to stress-release joints commonly observed in modern valley slopes (Figure 6).

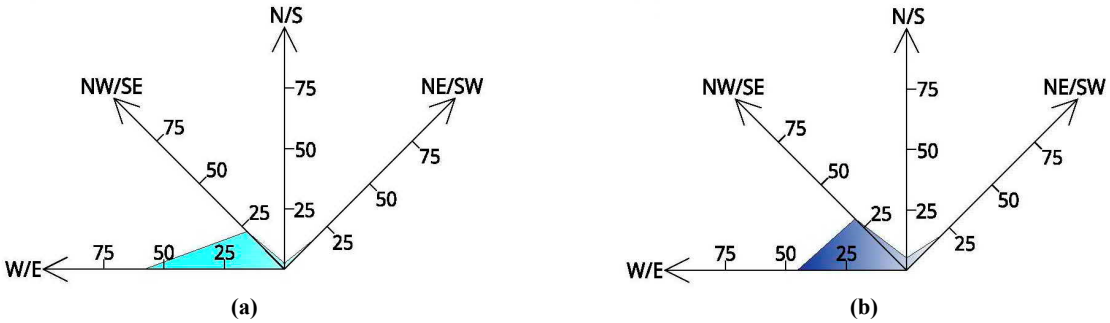

(a) (b)

Figure 9. Rose diagram of karst sinkhole orientation: for the Pivovarovsky karst area (a), for karst terrain No. 6 (b)

6. Discussion

The objective of this study was to develop an automated approach for karst susceptibility assessment, with a view to addressing several key challenges in the field of engineering geology and karst hazard forecasting. However, the successful application of this methodology requires consideration of several key conditions.

A primary challenge in karst assessment using remote sensing is the limitation imposed by data resolution, which can hinder the detection of smaller karst forms. The present study addressed

this issue by using high-resolution satellite imagery, which allows for the identification and mapping of even minor karst features with sufficient accuracy for regional analysis.

Furthermore, accurate karst hazard zoning along linear infrastructure requires precise geolocation of all mapped sinkholes. Consequently, the judicious selection of an appropriate coordinate system is imperative. A common methodological challenge in zoning by environmental conditions is the potential introduction of subjective judgement. In order to mitigate the potential consequences of this phenomenon, a strict set of zoning criteria was established and adhered to, with these criteria being tailored to the specific environmental factors of the region. The implementation of this objective framework was instrumental in ensuring the reproducibility of the zoning results, thereby minimizing the impact of analyst bias.

A significant concern when employing automated morphometric calculations on remote sensing-derived data is the need for robust result validation. This challenge was resolved by employing a study area (the Pivovarovo karst region) with a pre-existing, field-verified catalogue of karst forms. This facilitated direct comparison, during which our tool exhibited high accuracy, with calculated values for the major and minor axes demonstrating an 85-97% and 99-100% match with field measurements, respectively, and overall deviations not exceeding three meters.

The implementation of an automated approach has been demonstrated to yield substantial advantages. The automated zoning of the linear construction corridor in relation to sinkhole proximity provides an immediate visual indication of sectors susceptible to karst. Analyses of this nature, conducted at the planning stage, facilitate the expeditious implementation of design modifications. For instance, they may result in the recommendation of re-routing to circumvent the most hazardous karst areas.

Moreover, the zoning of the territory according to environmental conditions identifies homogenous areas where karst activity takes place uniformly and sinkholes are formed by analogous mechanisms. The accuracy of predictions of karst susceptibility within such zones is enhanced by the consideration of the heterogeneity of the karst massif. Consequently, normative estimates of karst sinkhole sizes are more reliable when constrained within these karst zonation taxa – individual karst terrains.

In areas where sinkholes are present in high numbers, manual measurement of diameters – whether conducted in situ or from imagery – is a laborious and time-consuming process. The custom-built instrument has been developed for the purpose of calculating the diameters of all karst sinkholes, which are identified through a combination of remote sensing interpretation and field observations. The instrument has been demonstrated to achieve this with a high degree of accuracy, and in a significantly reduced time frame. Beyond efficiency, automation ensures high precision in diameter estimation and enables the rapid processing of large datasets.

A further significant outcome of this study is the ability to determine the orientation of the major axis of sinkholes. The prevailing orientation pattern within a conditionally homogeneous area can be used to infer the direction of fracturing in the karst massif. It is imperative to comprehend the mechanisms governing this structural control, as fracture zones frequently delineate the emergence of new sinkholes. This understanding facilitates the identification of regions exhibiting a high susceptibility to sinkhole formation.

The methodology for surface karst research, integrating remote sensing data, field measurements and spatial analysis, is delineated in the flowchart (Figure 10). The diagram delineates the key procedural steps, from initial data collection to the final karst hazard zoning, thereby providing a clear overview of the methodological workflow.

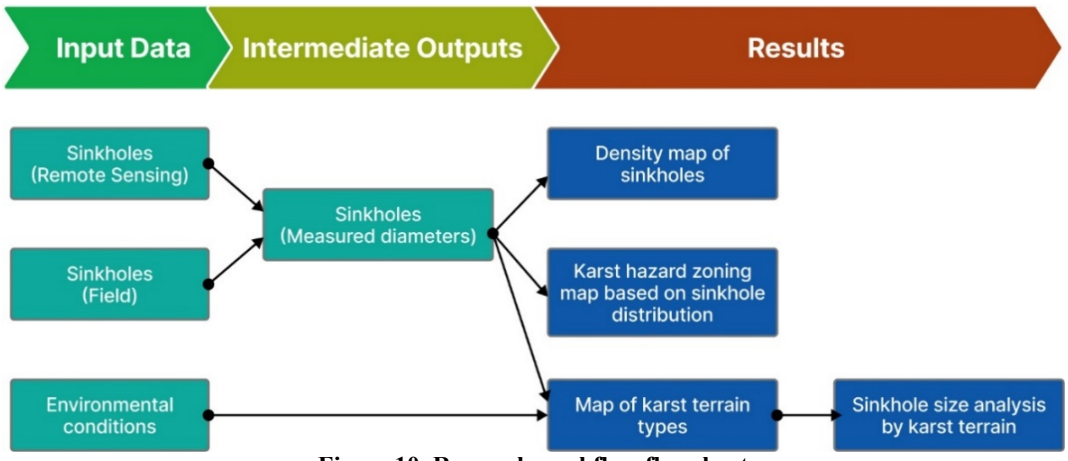

Figure 10. Research workflow flowchart

7. Conclusions

The study demonstrates that the application of standard geoinformation system tools, enhanced with custom ones, significantly advances karst susceptibility assessment for linear infrastructure. The approach is centred on a custom-developed Python algorithm for GIS that automates the morphometric analysis of karst forms. This tool efficiently calculates key parameters, including maximum and minimum diameters and the orientation of sinkholes, by processing a large number of input objects with high speed and accuracy, as validated by field data.

The integration of remote sensing data and geoinformation tools creates a powerful framework for advanced karst susceptibility assessment, enabling rapid and precise zoning of territories relative to sinkhole locations and zoning according to environmental conditions. The developed methodology is designed for transferability and can be implemented effectively in any karst region where clearly identifiable sinkholes are present. The integration of remote sensing data and field research geolocated data enhances the applicability of the approach in regions characterized by variable data availability and sinkhole sizes. The approach enables rapid, data-driven analysis, facilitating decision-making during the planning and design stages of engineering projects. This, in turn, facilitates the optimization of designed routes and the mitigation of karst-related risks.

Declaration of competing interest

There are no any competing financial, professional, or personal interests from other parties.

Acknowledgements

The research was supported by the Russian Science Foundation, grant No. 24-27-00350, https://rscf.ru/project/24-27-00350/.

References

[1]. Budiyanto, E., Muzayanah, & Prasetyo, K. (2020) Karst groundwater vulnerability and risk to pollution hazard in the Eastern part of Gunungsewu karst area. In IOP Conf. Series: *Earth and Environmental Science*, *412* 012020. https://doi.org/10.1088/1755-1315/412/1/012020

[2]. Sauro, U. (2003) Dolines and sinkholes: Aspects of evolution and problems of classification. *Acta Carsologica*, *32/2*(4), 41–52.

[3]. Theilen-Willige B. (2023) Overview of circular structures of various origins and sizes in Egypt as a contribution to natural hazard data mining based on remote sensing data and geoinformation systems (GIS) analysis. *Prevention and treatment of natural disasters*, *2*(2), 7–19. https://doi.org/10.54963/ptnd.v2i2.167

[4]. Sharma S., Parasar S.S., & Singh K. (2025) Multi-criteria decision modelling for forest fire risk mapping in protected areas of Mayurbhanj District, Odisha: A Case study in a geomorphologically diverse touristic landscape. *Ecological Questions 36*(3), 1–38. https://doi.org/10.12775/EQ.2025.030

[5]. Singh K., Sharma A., Tiwary A.K., Kaushal M., Nautiyal A., Gupta S.K., Sahoo S., Salem A., El-Hendawy S., Mattar M.A., Randeep, & Kansal R.B. (2025) A GIS-based study on groundwater level fluctuation and delineation of potential zones. *Environmental Earth Sciences*, *84,* 233. https://doi.org/10.1007/s12665-025-12197-1

[6]. Mahato P., Srivastava S., & Pandey S. (2025) Integrating AHP Decision-Making Tool for Landslide Susceptibility Zone Mapping: Insights from Mandi, Himachal Pradesh. *Operations Research Forum, 6*(4). https://doi.org/10.1080/23311916.2025.2530569

[7]. Dhakal D., Singh K., Kaur D., Verma S., Alsabhan A.H., Alam S., Al-sareji O.J., Randeep, & Kavita (2025) Landslide-induced vulnerability of road networks in Lahaul and Spiti, India: a geospatial study. *Bulletin of Engineering Geology and the Environment, 84*, 336. https://doi.org/10.1007/s10064-025-04328-6

[8]. Dhakal D., Singh K., Onyelowe K.C., Cazco S.A.S., Sharma A., Alarifi N., Islam F., Randeep, Arunachalam K.P., & Youssef M.Y. (2025). Enhancing landslide disaster prediction by evaluating non landslide area sampling in machine learning models for Spiti Valley India. *Scientific Reports*, *15*, 12242. https://doi.org/10.1038/s41598-025-95087-7

[9]. Bigdeli A., Maghsoudi A., & Ghezelbash R. (2024) A comparative study of the XGBoost ensemble learning and multilayer perceptron in mineral prospectivity modeling: a case study of the Torud-Chahshirin belt, NE Iran. *Earth Science Informatics*, *17*(1), 483-499. https://doi.org/10.1007/s12145-023-01184-4

[10]. Bigdeli A., Maghsoudi A., & Ghezelbash R. (2023). Recognizing geochemical anomalies associated with mineral resources using singularity analysis and random forest models in the Torud-Chahshirin Belt, Northeast Iran. *Minerals*, *13*(11), 1399. https://doi.org/10.3390/min13111399

[11]. Dhakal D., & Singh K. A Geospatial Approach to Landslide Susceptibility Mapping of Spiti, India. *Journal of Mining and Environment (JME), 16*(1), 2025, 183-205. https://doi.org/10.22044/jme.2024.14684.2779

[12]. Thakur, S., Tangri, A., Singh, K, Singh K, & Sharma S. (2025) Assessing Delhi Region's air quality using geospatial technologies: a comparative analysis of pollution trends during the COVID period (2018–2023). *Environmental Monitoring and Assessment*, *197*, 722. https://doi.org/10.1007/s10661-025-14177-1

[13]. Drobinina E.V., Kitaeva M.A., & Romanova E.R. (2025) Monitoring of hazardous geotechnical processes using the geoinformation systems and earth remote sensing data. *Bulletin of Perm University. Geology*, *24*(1), 23-31. https://doi.org/10.17072/psu.geol. 24.1.23

[14]. Orhan, O., Yakar, M., & Kırtıloglu O.S. (2017). A web based service application for visual sinkhole inventory information system; case study of Konya closed basin. *Selçuk Üniversitesi Mühendislik, Bilim Ve Teknoloji Dergisi*, *5*(1), 72-82. https://doi.org/10.15317/Scitech.2017.71

[15]. Ollivier C., Chalikakis, K., Mazzilli, N., Kazakis N., Lecomte, Y., Danquigny, Ch., & Emblanch, Ch. (2019) Challenges and limitations of karst aquifer vulnerability mapping based on the PaPRIKa method – application to a Large European Karst Aquifer (Fontaine de Vaucluse, France). *Environments*, *6*(3:39). https://doi.org/10.3390/environments6030039

[16]. Fiorillo, F., Pagnozzi, M., & Ventafridda, G. (2015) A model to simulate recharge processes of karst massifs. *Hydrological Processes*, *29* (10), 2301-2314. https://doi.org/10.1002/hyp.10353

[17]. Goldscheider, N. (2010). Delineation of spring protection zones. In N. Kresić & Z. Stevanović (Eds.), *Groundwater hydrology of springs* (pp. 305–338). Elsevier. https://doi.org/10.1016/B978-1-85617-502-9.00008-6

[18]. Goldscheider, N., Meiman, J., Pronk M., & Smart Ch. (2008) Tracer tests in karst hydrogeology and speleology. *International Journal of Speleology*, *37*(1), 27-40. https://doi.org/10.5038/1827-806X.37.1.3

[19]. Leone G., Catani V., Pagnozzi M., Ginolfi M., Testa G., Esposito L., & Fiorillo F. (2022) Hydrological features of Matese Karst Massif, focused on endorheic areas, dolines and hydroelectric exploitation. *Journal of Maps*, *19*(1), 1-13. https://doi.org/10.1080/17445647.2022.2144497

[20]. Polyakova E.V., Kutinov Y.G., Mineev A.L., Chistova, Z.B., Belenovich, & T.Ya. (2021) Using the ASTER GDEM v.2 global digital elevation model to identify areas of possible activation of karst processes in the Arkhangelsk region (Russia). *Uchenye Zapiski Kazanskogo Universiteta. Seriya Estestvennye Nauki*, *163*(2), 302-319. https://doi.org/10.26907/2542-064X.2021.2.302-319

[21]. Carvalho Júnior, O.A de., Guimarães, R.F., Montgomery, D.R., Gillespie, A.R., Gomes, R.A.T., Martins, É.d.S., & Silva, N.C. (2014) Karst depression detection using ASTER, ALOS/PRISM and SRTM-Derived digital elevation models in the Bambuí Group, Brazil. *Remote Sensing*, *6*, 330-351 https://doi.org/10.3390/rs6010330

[22]. Garas, K.L., Madrigal, M.F.B., Agot, R.D.D., Canlas, M.C.M., & Manzano, L.S.J. (2020) Karst depression detection using IFSAR-DEM: a tool for subsidence hazard assessment in Panglao, Bohol. *Carsologica Sinica*, *39*(6), 928-936.

[23]. Hofierka, J., Gallay, M., Bandura, P., & Šašak, J. (2018) Identification of karst sinkholes in a forested karst landscape using airborne laser scanning data and water flow analysis. *Geomorphology*, *308*, 265-277. https://doi.org/10.1016/j.geomorph.2018.02.004

[24]. Kobal, M., Bertoncelj, I., Pirotti, F., Dakskobler, I., & Kutnar, L. (2015) Using lidar data to analyse sinkhole characteristics relevant for understory vegetation under forest cover – case study of a high karst area in the dinaric mountains. *PLoS One*, *10*(3), article e0122070. https://doi.org/10.1371/journal.pone.0122070

[25]. Yu, B., Zhang, T., Zheng, K., Zuo, S., Han, X., Wang, S., & Chen, S. (2023). Enclosed karst depression identification and analysis for the pumped storage power station reservoir construction using DEM. *Geofluids*, Article 4794665. https://doi.org/10.1155/2023/4794665

[26]. Gokkaya, E., Gutierrez, F., Ferk, M., & Gorum, T. (2021) Sinkhole development in the Sivas gypsum karst, Turkey. *Geomorphology, 386*(5):107746. https://doi.org/10.1016/j.geomorph.2021.107746

[27]. Doneus, M. (2013) Openness as visualization technique for interpretative mapping of airborne lidar

derived digital terrain models. *Remote Sensing, 5*(12), 6427-6442. https://doi.org/10.3390/rs5126427

[28]. Drobinina, E.V. (2022) Automation of surface karst assessment using Sentinel-2 satellite imagery. *Sovremennye problemy distantsionnogo zondirovaniya Zemli iz kosmosa*, *19*(6), 79-90. https://doi.org/10.21046/2070-7401-2022-19-6-79-90

[29]. Erofeev, E.A., & Kataev, V.N. (2017) Identification of surface karst forms on satellite data. In: Collection of Scientific Articles, *Geology and Mineral Resources of the Western Urals*, *3*(16), 193-197. http://dx.doi.org/10.17072/psu.geol.16.3.300

[30]. Vakhrushev, B., Kunov, A., & Kunov, V. (2022) Using the method of decoding satellite images in order to map surface karst forms and subsequent spatial analysis of the nature of their placement. *Scientific notes of V.I. Vernadsky Crimean federal university. Geography. Geology*, *8*(74), 4, 248-263.

[31]. Oosthuizen, A., & van Rooy, J. (2015) Hazard of sinkhole formation in the Centurion CBD using the Simplified Method of Scenario Supposition. *Journal of the South African Instiution of Civil Engineering*, *57*(2), 69-75. https://doi.org/10.17159/2309-8775/2015/v57n2a8

[32]. Eduardo, O., Manchola, P., & Morais, F. (2023) Morphometric characterization of doliniform features in the Araguaia Plain *Sociedade & Natureza*, *35*(1). https://doi.org/10.14393/SN-v35-2023-67351x

[33]. Gantov, B. A. (2005). *Monitoring of the area of active karst formation near the village of Pivovarovo, Vyaznikovsky district, Vladimir region* (Report). Dzerzhinsk, Russia. (Archival materials)

[34]. Erofeev, E. A., & Kataev, V. N. (2010) Using probabilistic and statistical methods for estimating karst hazard assessment under conditions of anthropogenic influence on karst areas. *Engineering Geology World*, *4*, 34-46.

[35]. Tolmachev V. V. (1980) Probabilistic approach to the assessment of karst area stability and designing of antikarst constructions. *Engineering Geology World*, *3*, 98-107.

[36]. Gordienko, S. G., & Savelieva, Y. Y. (2001) Probabilistically statistical forecast of suffusion sinkholes formation in the drainage zone (by the example of Nizhegorodskaya hydropower station). *Proceedings of the VNIIG*, *239*, 119-124.

[37]. Selina, Z. V., & Kovaleva, T. G. (2023) Probability of formation of new karst forms near existing forms. In: Collection of Scientific Articles, *Geology and Mineral Resources of the Western Urals*, *6*(43), 295-299.

[38]. Kostarev, V. P. (1979) On quantitative indicators of karst and their use in engineering geological assessment of karst territories. *Engineering construction surveys*, *1*(53), 49-53.

[39]. Soltanpour, H., Serrhini, K., Gill, J.C., Fuchs, S., & Mohadjer S. (2024) Multi-hazard susceptibility mapping in the karst context using a machine-learning method (MaxEnt). *EGUsphere* [Preprint]. https://doi.org/10.5194/egusphere-2024-1779

[40]. Savarensky, I. A. (1990). Forecasting territory stability using the distance-from-nearest-karst-manifestation method. In *Forecast of changes in engineering-geological conditions during construction: Collection of scientific works* (pp. 108–118). Nauka.

[41]. Shcherbakov, S. V., & Zolotarev, D. R. (2008). Prediction of stability of karst territories (on the example of Kungur city). In *Proceedings of the 2008 Conference of Students, Postgraduates and Young Scientists of the Department of Geology: Geology in the developing world* (pp. 164–168). Perm State University.

[42]. Production and Research Institute for Engineering Surveys in Construction [PNIIIS] & Gosstroy of Russia. (2001). *Engineering geological site investigations for construction* (Code of Rules 11-105-97).

[43]. Bosak, P. (2008) Karst processes and time, *Geologos*, *14*, 19-36.

[44]. Xingli, J., Qingmiao, D., & Hongzhi, Y. (2020). Susceptibility zoning of karst geological hazards using machine learning and cloud model. *Cluster Computing, 22*(4, Suppl.), S8051–S8058. https://doi.org/10.1007/s10586-017-1590-0

[45]. Gao, L., Shi, Y., Qiu, Y., Ma, C., & Zhou, A. (2023) The analyses of land use and prevention in high-density main urban areas under the constraint of karst ground subsidence: study of Wuhan city, China. *ISPRS International Journal of Geo-Information*, *12*, 425. https://doi.org/10.3390/ijgi12100425

[46]. Yang, Y., Ma, X., Ding, W., Wen, H., & Sun, D. (2024) A novel dataset replenishment strategy integrating time-series INSAR for refined landslide susceptibility mapping in karst regions. *Water*, *16*, 2414. https://doi.org/10.3390/w16172414

[47]. Popov, I. V. (1959). *Inzhenernaya geologiya* [Engineering geology]. Moscow State University.

[48]. Sergeev, E. M. (1978). *Inzhenernaya geologiya* [Engineering geology]. Moscow State University.

[49]. Kataev, V. N. (2001). *Metodologiya i praktika sravnitel'no-otsenochnogo karstovogo rayonirovaniya* [Methodology and practice of comparative evaluation karst zoning]. Perm State University.

[50]. Kitaeva, M. A., & Drobinina, E. V. (2023) Experience of karst zoning of the linear construction design territory, S*peleology and speleostology*, *2*, 21-26.

[51]. Zolotarev, D. R. (2012) The results of lineament analysis on the karst areas of Permsky krai, *Modern problems of science and education*, *5*, 345-345

[52]. Zolotarev, D. R., & Kataev, V. N. (2013) Lineament tectonic influence on development of karst processes at the local level. *Georisk*, *1*, 34-43.

انجمن مهندسی معدن ایران
نشریه مهندسی معدن و محیط زیست
نشانی نشریه: www.jme.shahroodut.ac.ir
دانشگاه صنعتی شاهرود

ارزیابی حساسیت کارست در تاسیسات زیرساخت خطی با استفاده از GIS و سنجش از دور در منطقه ولادیمیر، روسیه

النا دروبینا[۱]*، مارینا کیتاوا[۱]، آرتم میزف[۱] و الیزاوتا رومانوا[۲،۳]

۱. دانشکده زمین شناسی، دانشگاه ایالتی پرم، پرم، فدراسیون روسیه
۲ .موسسه سرگیف علوم زمین زیست محیطی آکادمی علوم روسیه، مسکو، فدراسیون روسیه
۳. دانشگاه دولتی مهندسی عمران مسکو (MGSU) دانشگاه ملی تحقیقاتی مسکو، فدراسیون روسیه

اطلاعات مقاله

تاریخ ارسال: ۲۰۲۵/۱۰/۲۹
تاریخ داوری: ۲۰۲۵/۱۲/۰۱
تاریخ پذیرش: ۲۰۲۵/۱۲/۲۰

DOI:10.22044/jme.2025.17055.3363

کلمات کلیدی

GIS
کارست
حساسیت کارستی
داده‌های سنجش از دور
فروچاله

چکیده

این مطالعه یک رویکرد یکپارچه برای ارزیابی حساسیت کارست با استفاده از داده‌های سیستم‌های اطلاعات جغرافیایی (GIS) و سنجش از دور (RS) برای نقشه‌برداری فروچاله و تحلیل فضایی ارائه می‌کند. این رویکرد ارزیابی حساسیت کارست سریع و قابل اعتماد را در مناطقی که زیرساخت های خطی در منطقه کارست پیووارووو (منطقه ولادیمیر، روسیه) طراحی شده است، امکان پذیر می کند. این تحقیق مزایای منطقه بندی خودکار در طول مسیر ساخت و ساز را بر اساس توزیع چاله و شرایط محیطی برجسته می کند. یک سهم روش‌شناختی قابل توجه در ارزیابی حساسیت کارست، توسعه یک ابزار سفارشی مبتنی بر پایتون برای تجزیه و تحلیل مورفومتریک خودکار فروچاله‌ها، از جمله اندازه‌گیری قطر و ارزیابی جهت‌گیری است. این رویکرد یک راه حل موثر برای ارزیابی حساسیت کارست فراهم می کند، زیرا پردازش سریع مجموعه داده های بزرگ را امکان پذیر می کند و نتایج با کیفیت بالا تولید می کند که می تواند از تصمیمات طراحی مهندسی پشتیبانی کند.

نویسنده مسئول مکاتبات: *alenadrobinina@yandex.ru* (الف. دروبینا)